Importance of Matrix Element Effects in the Scanning Tunneling Spectra of High-Temperature Superconductors

Jouko Nieminen[1,2],* Hsin Lin[2], R.S. Markiewicz[2], and A. Bansil[2]
[1]*Institute of Physics, Tampere University of Technology, P.O. Box 692, 33101 Tampere, Finland and*
[2]*Physics Department, Northeastern University, Boston, Massachusetts 02115*
(Dated: Version of May 12, 2008)

We have developed a material specific theoretical framework for modelling scanning tunneling spectroscopy (STS) of high temperature superconducting materials in the normal as well as the superconducting state. Results for $Bi_2Sr_2CaCu_2O_{8+\delta}$ (Bi2212) show clearly that the tunneling matrix element strongly modifies the STS spectrum from the LDOS of the $d_{x^2-y^2}$ orbital of Cu. The dominant tunneling channel to the surface Bi involves the $d_{x^2-y^2}$ orbitals of the four neighbouring Cu atoms. In accord with experimental observations, the computed spectrum displays a remarkable asymmetry between the processes of electron injection and extraction, which arises from contributions of Cu d_{z^2} and other orbitals to the tunneling current.

PACS numbers: 68.37.Ef 71.20.-b 74.50.+r 74.72.-h

Scanning tunneling spectroscopy (STS) has entered the realm of high-temperature superconductors powerfully by offering atomic scale spatial resolution in combination with high energy resolution. The physics of these materials is dominated by the cuprate layers, which are usually not exposed to the tip of the apparatus. Much of the existing interpretation of the spectra is based however on the assumption that the STS spectrum is directly proportional to the local density of states (LDOS) of the CuO_2 layer, neglecting the effects of the tunneling matrix element in the presence of the insulating overlayers. Here, we focus on the Bi2212 system, which has been the subject of an overwhelming amount of experimental work[1, 2, 3, 4, 5], although our results bear more generally on the STS spectra of the cuprates. We take into account the fact that the current originating in the CuO_2 layers reaches the tip after being 'filtered' through the overlayers of SrO and BiO, and show that instead of being a simple reflection of LDOS of the CuO_2 layers, the STS signal represents a complex mapping of the electronic structure of the system.

In order to construct a realistic framework capable of describing the tunneling spectrum of the normal as well as the superconducting state of the cuprates, we start with the normal state Hamiltonian

$$\hat{H}_1 = \sum_{\alpha\beta\sigma} \left[\varepsilon_\alpha c^\dagger_{\alpha\sigma} c_{\alpha\sigma} + V_{\alpha\beta} c^\dagger_{\alpha\sigma} c_{\beta\sigma} \right], \qquad (1)$$

which describes a system of tight-binding orbitals created (or annihilated) via the real-space operators $c^\dagger_{\alpha\sigma}$ (or $c_{\alpha\sigma}$). Here α is a composite index denoting both the type of orbital (e.g. Cu $d_{x^2-y^2}$) and the site on which this orbital is placed, and σ is the spin index. ϵ_α is the on-site energy of the α^{th} orbital. α and β orbitals interact with each other through the potential $V_{\alpha\beta}$ to create the energy eigenstates of the entire system.

Superconductivity is included by adding a pairing interaction term Δ in the Hamiltonian of Eq. 1 as follows

$$\hat{H} = \hat{H}_1 + \sum_{\alpha\beta\sigma} \left[\Delta_{\alpha\beta} c^\dagger_{\alpha\sigma} c^\dagger_{\beta-\sigma} + \Delta^\dagger_{\beta\alpha} c_{\beta-\sigma} c_{\alpha\sigma} \right] \qquad (2)$$

We take Δ to be non-zero only between $d_{x^2-y^2}$ orbitals of the nearest neighbor Cu atoms, and to possess a d-wave form, i.e. Δ is given in momentum space by $\Delta_k = \frac{\Delta}{2}\left[\cos k_x a - \cos k_y a\right]$, where a is the in-plane lattice constant. This interaction allows electrons of opposite spin to combine into superconducting pairs such that the resulting superconducting gap is zero along the nodal directions $k_x = \pm k_y$, and is maximum along the antinodal directions.

The Bi2212 sample is modeled as a slab of seven layers in which the topmost layer is BiO, followed by layers of SrO, CuO_2, Ca, CuO_2, SrO, and BiO, as shown in

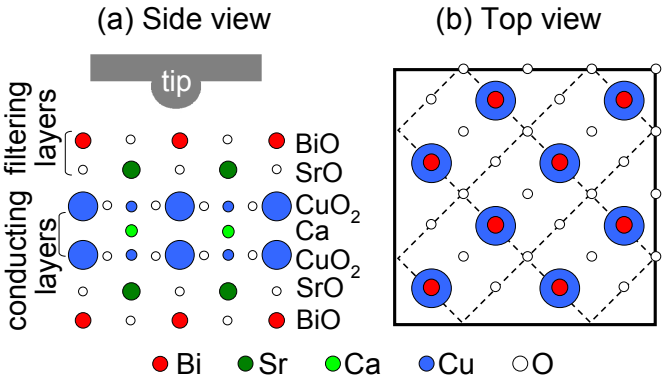

FIG. 1: (a) Side view showing tip placed schematically on top of seven layers used to compute the tunneling spectrum of Bi2212, where the surface terminates in the BiO layer. Tunneling signal from the conducting CuO_2 layers reaches the tip after passing through the filtering layers of SrO and BiO. (b) Top view of the surface showing the arrangement of various atoms. Eight two-dimensional real space primitive unit cells used in the present computations are marked by dashed lines.

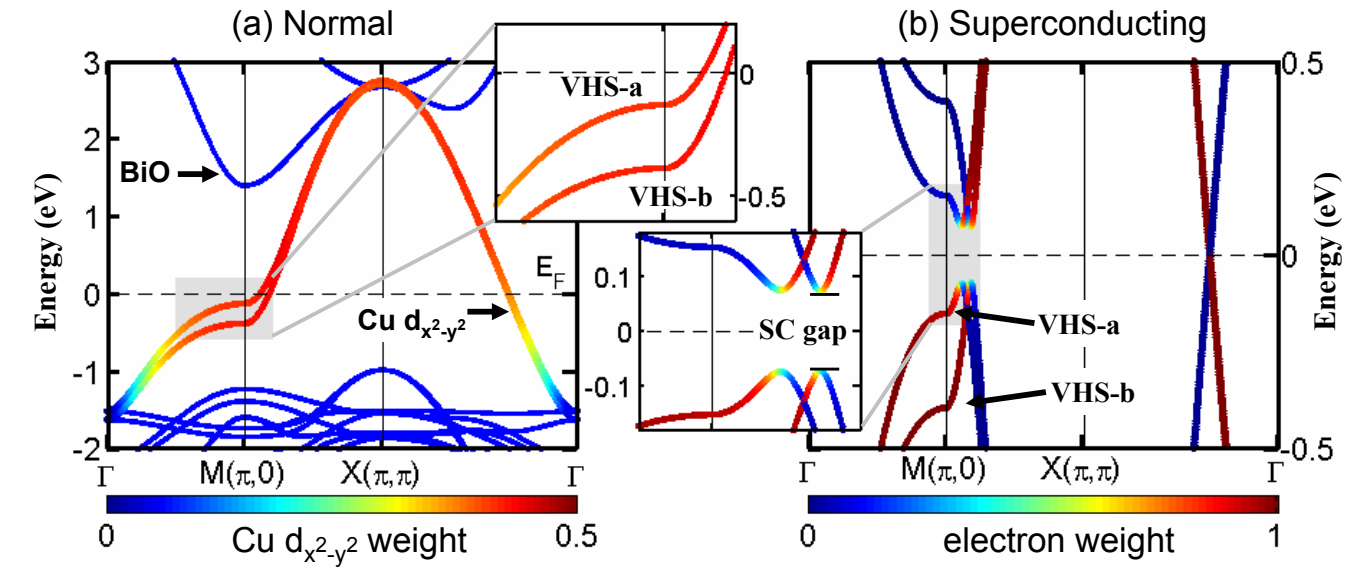

FIG. 2: (a) Normal state electronic spectrum of Bi2212. Cu $d_{x^2-y^2}$ weight of states is given by the color of the dots. Inset shows the energy region of the VHS's on an expanded scale. (b) Electronic spectrum of the superconducting state. Electron weight of states is given by the color of the dots. Inset highlights the region of the superconducting gap near the antinodal point.

Fig. 1(a). The tunneling computations are based on a $2\sqrt{2} \times 2\sqrt{2}$ real space supercell consisting of 8 primitive surface cells with a total of 120 atoms (see Fig. 1(b)). The coordinates are taken from the tetragonal crystal structure of Ref. 6. A tetrahedral cluster of atoms attached to a thin slab simulates the tip and tip holder. The tip is allowed to scan across the substrate to generate the topographic STM map, or held fixed on top of a surface Bi atom for the STS spectra.

The tight-binding parameters are fitted to the LDA band structure of Bi2212 that underlies for example the extensive angle-resolved photointensity computations of Ref. 7. The Slater-Koster results[8, 9] are used to fix the angular dependence of the tight binding overlap integrals. The specific orbital sets used for various atoms are: (s, p_x, p_y, p_z) for Bi and O; s for Sr; and $(4s, d_{3z^2-r^2}, d_{xy}, d_{xz}, d_{yz}, d_{x^2-y^2})$ for Cu atoms. This yields 58 orbitals in a primitive cell, used in band calculations, and a total of 464 orbitals for Green function supercell calculations in 256 evenly distributed k-points. Finally a, gap parameter value of $|\Delta| = 0.045eV$ is chosen to model a typical experimental spectrum[1] for the generic purposes of this study.

The LDOS and tunneling computations are based on Green function formalism. At first, the normal-state Green function is constructed via Dyson's equation using methodology described in Ref. 10. At this stage a self-energy for orbital α, $\Sigma^{\pm}_{\alpha} = \Sigma'_{\alpha} \pm i\Sigma''_{\alpha}$ is embedded in Dyson's equation for possible effects of various bosonic couplings and correlation effects [11, 12]. For simplicity, we have assumed the self-energy to be diagonal in the chosen basis. In building up the Green function in the superconducting state, we utilize the conventional BCS-type self-energy $\Sigma^{BCS} = \Delta G^h \Delta^{\dagger}$ (see, e.g., Ref. 13), where G^h is the hole part of normal state Green function.

Fig. 2 shows the calculated band structure of Bi2212 in the normal as well as the superconducting state from Hamiltonians of Eqs. 1 and 2. The normal state is seen to properly display the major features such as: The pair of CuO_2 bands crossing the Fermi energy (E_F) with the associated van Hove singularities (VHS's) marked VHS-a (antibonding) and VHS-b (bonding), split by 250 meV at the $(\pi, 0)$ point; BiO bands lying about 1 eV above E_F; and the 'spaghetti' of bands involving various Cu and O orbitals starting at a binding energy of around 1 eV below E_F. Although states near E_F are mainly of Cu $d_{x^2-y^2}$ and O $p_{x,y}$ character, they also contain some Bi and Cu d_{z^2} admixture. In the superconducting state in Fig. 2(b), a quasiparticle spectrum mirrored through E_F is obtained with a doubled number of bands due to the pairing interaction. A d-wave superconducting gap opens up in both CuO_2 bands near E_F. The quasiparticles have a mixed electron/hole character only near the edges of the gap.

To compute the tunneling spectra we apply the Todorov-Pendry expression [14, 15] for the differential conductance σ between orbitals of the tip (t, t') and the sample(s, s'), which in our case yields

$$\sigma = \frac{dI}{dV} = \frac{2\pi e}{\hbar} \sum_{tt'ss'} \rho_{tt'}(E_F) V_{t's} \rho_{ss'}(E_F + eV) V^{\dagger}_{s't}, \quad (3)$$

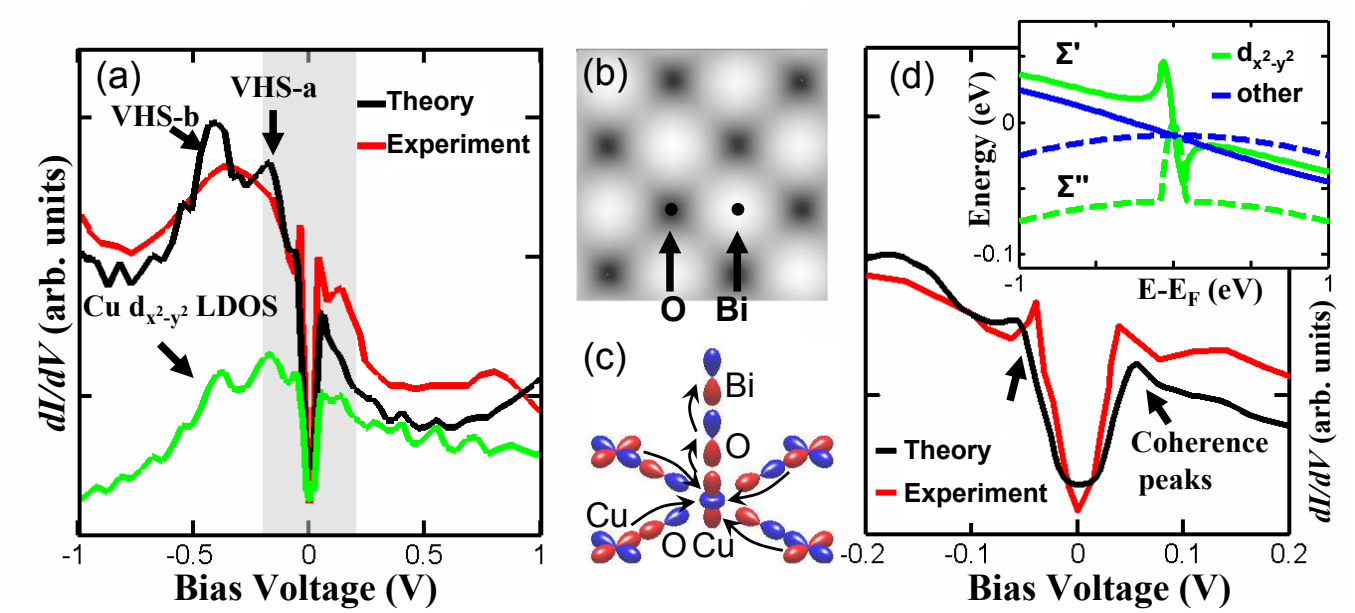

FIG. 3: (a) Computed (black line) and experimental (red line) differential tunneling spectra, dI/dV, as a function of bias voltage (in volts). Local density of states (LDOS) of Cu $d_{x^2-y^2}$ electrons is shown (green line) as a function of energy, where the horizontal scale is in eV. (b) Computed topographic image of the BiO surface in which Bi atoms are bright and O atoms are dark. (c) The main tunneling channel from Cu $d_{x^2-y^2}$ electrons on nearest neighbor Cu atoms to the tip through overlap with the central Cu atom, followed by hopping to the p_z orbitals of the apical O-atom and the Bi atoms. (d) Computed and measured spectra in the low energy region marked by gray shading in (a). Inset gives the real (solid lines) and imaginary (dashed lines) parts of the self-energy applied to the Cu $d_{x^2-y^2}$ states and to all other states.

where the density matrix $\rho_{ss'} = -\frac{1}{\pi}\sum_\alpha G^+_{s\alpha}\Sigma''_\alpha G^-_{\alpha s'}$ is, in fact, the spectral function written in terms of retarded/advanced Green function and the self-energy. Eq. 3 differs from the more commonly used Tersoff-Hamann approach[16] in that it takes into account the details of the symmetry of the tip orbitals and their overlap with the surface orbitals.

The use of the spectral function recasts Eq. 3 into the form

$$\sigma = \sum_{t\alpha} T_{t\alpha}, \tag{4}$$

where

$$T_{t\alpha} = -\frac{2e}{\hbar}\sum_{t's s'} \rho_{tt'}(E_F) V_{t's} G^+_{s\alpha}\Sigma''_\alpha G^-_{\alpha s'} V^\dagger_{s't}, \tag{5}$$

and the Green functions and the self-energy are evaluated at energy $E = E_F + eV_b$. Eq. 5 is similar to the Landauer-Büttiker formula for tunneling across nanostructures (see, e.g., Ref. 17), and represents a slight reformulation of Refs. 18 and 19.

The nature of Eq. 5 can be understood straightforwardly: $G_{s\alpha}$ gives the amplitude with which electrons residing on the α^{th} orbital in the solid propagate to the surface at energy E broadened by Σ''_α. The term V_{st} is the overlap between the surface orbital and the tip, while $\rho_{tt'}$ gives the available states at the tip. Hence, $T_{t\alpha}$ gives the contribution of the α^{th} orbital to the current, and the summation in Eq. 4 collects these individual contributions to yield the total tunneling current which reaches the tip. Thus, selecting individual terms in Eq. 5 provides a transparent scheme to define tunneling paths between the sample and the microscope tip.

Fig. 3(a) shows the tunneling spectra over the broad energy range of ± 1 eV. At high positive voltages, the computed spectrum (black line) is fairly structureless. At low energies, a gap accompanied by the characteristic peak-dip-hump features is observed. The calculations show the anti-bonding (VHA-a) and bonding (VHS-b) VHS's[12] as distinct structures, followed by a broad dip around -0.7 eV and subsequent rise near -1 eV. In all these respects the present calculations follow the experiment (red line) of Ref. [1]. Moreover, theory reproduces the observed asymmetry of the tunneling spectrum with excess intensity at negative biases. The rapid increase in current at high binding energies results from increasing spectral weight of Cu d_{z^2} and other orbitals contributing to the 'spaghetti' of bands starting around 1 eV binding energy (see Fig. 2(a)). We emphasize that the LDOS of the Cu $d_{x^2-y^2}$ (green line in Fig. 3(a)) does not provide a good description of the spectrum. In particular, the Cu $d_{x^2-y^2}$ LDOS possesses an asymmetry which is opposite to that of the tunneling spectrum.

Fig. 3(d) gives a blow up of the low energy region of $\pm 0.2eV$, shown by gray shading in Fig. 3(a). The

computed spectrum is seen to reproduce the coherence peaks and the characteristic peak-dip-hump feature. The generic form of the real and imaginary parts of the self-energies applied to the Cu $d_{x^2-y^2}$ orbitals (solid and dashed blue lines, respectively) and the rest of the orbitals are given in the inset. Fig. 3(b) shows the computed 'topographic map' of the BiO surface in constant current mode. Bi atoms appear as bright spots in accord with experimental observations, while O atoms sit at the centers of dark regions.

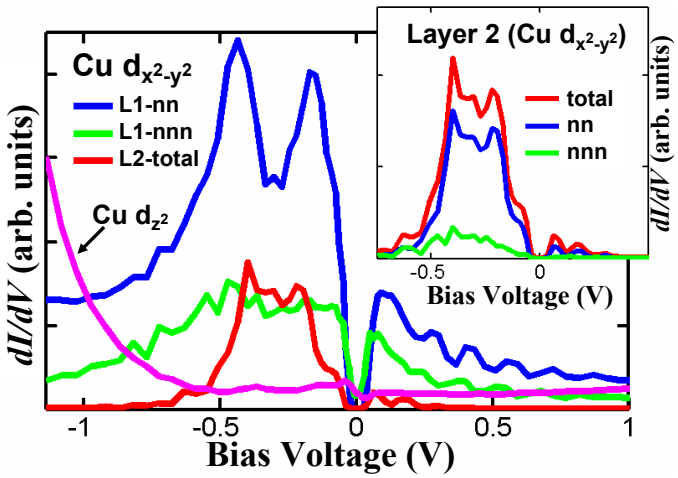

FIG. 4: *Main frame*: Partial contributions to the tunneling current from various orbitals in the two cuprate layers. The CuO_2 layer closest to the tip is identified as layer 1 or L1, while the second layer is denoted by L2. Specific contributions are: $d_{x^2-y^2}$ orbitals of the four nearest neighbor Cu atoms (L1-nn, blue line); $d_{x^2-y^2}$ orbitals of the four next nearest neighbor Cu atoms of the first layer (L1-nnn, green line) ; $d_{x^2-y^2}$ orbitals of the Cu atoms of the second layer (L2, red line); d_{z^2} of the central Cu atom of L1 (magenta line). *Inset*: Decomposition of the current from the second cuprate layer: Total contribution (red line); contribution of the four nearest neighbours (blue line); and the next nearest neighbours (green line).

An analysis of the partial terms of Eq. 5 reveals that the $d_{x^2-y^2}$ orbital of the Cu atom lying right under the Bi atom gives zero contribution to the current [20]. The dominant contribution to the spectrum comes from the four nearest neighbor (NN) Cu atoms as indicated schematically in Fig. 3(c). A detailed decomposition of Eq. 4 is shown in Fig. 4, where paths starting from the CuO_2 layer closest to the tip (L1), as well as from the second cuprate layer (L2) are considered. The signal from cuprate layers is dominated by the $d_{x^2-y^2}$ orbitals on the four nearest neighbour (nn) Cu atoms in L1 up to about -0.7 eV (blue line). At higher binding energies, the contribution from the d_{z^2} electrons from the Cu atom right below the Bi atom or the tip grows rapidly (magenta line).

A smaller but still significant contribution comes from the four next nearest neighbour (nnn) $d_{x^2-y^2}$ orbitals in L1 spread over a wide energy range (green line, main figure), while the total current originating from the $d_{x^2-y^2}$ orbitals of L2 is quite localized over zero to -0.6 eV bias (red line, main figure). Fig. 4 emphasizes the nature of the current associated with the cuprate layers and points out an intrinsic electron-hole asymmetry originating from the d_{z^2} orbitals. We note however that the Bi and O orbitals in the surface Bi-O layer can also play a role in producing an asymmetric background current.

In conclusion, we find that STS spectrum for Bi2212 is strongly modified from the LDOS of $d_{x^2-y^2}$ by the effect of the tunneling matrix element. Much of the observed asymmetry of the spectrum can be explained within the conventional picture due to the turning on of Cu d_{z^2} and other channels with increasing (negative) bias voltage. This indicates that the effects of strong electronic correlations on the tunneling spectrum are more subtle than has been thought previously. However, we should note that we have not analyzed spectra associated with the deeply underdoped regime where charge order has been reported [21]. The present method naturally allows an analysis of the tunneling signal in terms of the possible tunneling channels and the related selection rules. Our scheme can be extended to incorporate effects of impurities and various nanoscale inhomogeneities by using appropriately larger basis sets in the computations.

Acknowledgments

This work is supported by the US Department of Energy, Office of Science, Basic Energy Sciences contract DE-FG02-07ER46352, and benefited from the allocation of supercomputer time at NERSC, Northeastern University's Advanced Scientific Computation Center (ASCC), and the Institute of Advanced Computing, Tampere.

* Electronic address: jouko.nieminen@tut.fi

[1] K. McElroy *et al.*, *Science* **309**, 1048 (2005).
[2] E.W. Hudson *et al.*, *Nature* **411**, 920 (2001).
[3] A.N. Pasupathy *et al.*, Science **320**, 196 (2008).
[4] A.V. Balatsky *et al.*, *Rev. Mod. Phys.* **78**, 373 (2006).
[5] Ø. Fischer *et al.*, *Rev. Mod. Phys.* **79**, 353(2007).
[6] V. Bellini, F. Manghi, T. Thonhauser, and C. Ambrosch-Draxl, *Phys. Rev. B* **69**, 184508(2004).
[7] H. Lin, S. Sahrakorpi, R.S. Markiewicz, and A. Bansil, *Phys. Rev. Lett.* **96**, 097001 (2006).
[8] J.C. Slater and G.F. Koster, *Phys. Rev.* **94**, 1498 (1954).
[9] W.A. Harrison, *Electronic Structure and Properties of Solids.* Dover, New York (1980).
[10] J.A. Nieminen and S. Paavilainen, *Phys. Rev. B* **60**, 2921 (1999).
[11] B.W. Hoogenboom, C. Berthod, M. Peter, O. Fischer, and A.A. Kordyuk, *Phys. Rev. B* **67**, 224502(2003).
[12] G. Levy de Castro *et al.*, *cond-mat/0703131* (2007).
[13] A.L. Fetter and J.D. Walecka, *Quantum Theory of Many-Particle Systems.* Dover (2003).
[14] T.N. Todorov *et al.*, *J.Phys.: Condens. Matter* **5**, 2389 (1993).

[15] J.B. Pendry *et al.*, *J.Phys.: Condens. Matter* **3**, 4313 (1991).
[16] J. Tersoff and D.R. Hamann, *Phys. Rev. B* **31**, 805 (1985).
[17] Y. Meir and N.S. Wingreen, *Phys. Rev. Lett.* **68**, 2512 (1992).
[18] H. Ness and A.J. Fisher, *Phys. Rev. B* **56**, 12469 (1997).
[19] T. Frederiksen, M. Paulsson, M. Brandbyge, and A.-P. Jauho, *Phys. Rev. B* **75**, 205413 (2007).
[20] I. Martin *et al.*, *Rev. Lett.* **88**, 097003 (2002).
[21] Y. Kohsaka *et al.*, *Science* **315**, 1380 (2007).